Exo-iron centres linked to MoFeS clusters

Frédéric Barrière,[a,b] **David J. Evans,**[a] **David L. Hughes,**[a] **Saad K. Ibrahim,**[a] **Jean Talarmin**[b] **and Christopher J. Pickett**[a]*

[a] *The Nitrogen Fixation Laboratory, John Innes Centre, Norwich Research Park, Colney, Norwich, UK NR4 7UH. E-mail: chris.pickett@bbsrc.ac.uk*
[b] *UMR CNRS 6521, Faculté des Sciences, Université de Bretagne Occidentale, BP 809, 29285 Brest, France*

Monocubane clusters with exo-iron atoms were synthesized from the iron-bridged dicubane $[NEt_4]_3[Mo_2Fe_7S_8(SEt)_{12}]$ by reactions with π-acid ligands. The structures of two derivatives, $[NEt_4][MoFe_3S_4X_3(\mu\text{-}SEt)_3Fe(CN^tBu)_3]$, X = Cl or PhS, have been established by X-ray crystallography. Electrochemical and Mössbauer data showed that the cubane core retains the $\{MoFe_3S_4\}^{3+}$ redox level of the parent material and that the exo-iron centre is in the low-spin iron(II) state. Infrared and electrochemical data showed that there is little electronic interaction between the cubane and exo-iron centres. The parent complex possesses a low-spin bridging iron(III) centre. This centre undergoes slow electron transfer which is ascribed to spin-state reorganisation to high-spin Fe^{II}. Reduction of the cubane units leads to reversible deco-ordination of a bridging thiolate group from a molybdenum centre.

Introduction

Studies of the electronic, magnetic and molecular structures of synthetic FeS, MoFeS, VFeS and other heterometallic FeS clusters, together with knowledge of their chemical and electrochemical properties, underpin our current, but far from complete, understanding of the structure and function of metallosulfur clusters in biology.[1,2] A key aspect of metallosulfur cluster chemistry is how redox changes within a cluster system affect the reactivity of Fe or heteroatoms contained within the clusters, as in the FeMo cofactor of nitrogenase, or of metal centres which are linked exogenously to metallosulfur assemblies, as in carbon monoxide dehydrogenase and nickel iron hydrogenase.[3]

In this paper we describe new, structurally characterised, monocubanes possessing exo-iron centres linked to the cubane unit by thiolate bridges to Mo. Surprisingly, spectroscopic and electrochemical evidence suggests that changing the ligands which substitute the exo-iron centre has a neglible electronic effect on the cubane core. Equally, substituent changes on the cubane Fe atoms have a negligible effect on the electronic condition of the exo-iron atom. Taken together, these results indicate that it is possible to construct bifunctional centres, which are spatially closely linked, but which intrinsically behave as electronically distinct units. This may be of some pertinence to the transmission of electronic effects in biological assemblies.

The iron thiolate bridged dicubane $[NEt_4]_3[Mo_2Fe_7S_8(SEt)_{12}]$ (**1** in Scheme 1) is the synthetic font of nearly all MoFeS monocubanes,[1,4–7] including the new complexes described herein. The electron-transfer chemistry of this molecule has been previously discussed.[5] We now show that the central iron atom undergoes slow electron-transfer chemistry, reversible reduction of both cubane sub-units can be observed at low temperature, and that the chemistry following electron transfer is probably associated with the opening of thiolate bridging ligands.

Results and discussion

Monocubanes with exo-iron centres

Synthesis and structures. The dicubane $[NEt_4]_3[Mo_2Fe_7S_8$-$(SEt)_{12}]$ **1** reacts slowly with CN^tBu in MeCN to afford $[NEt_4]$-$[MoFe_3S_4(SEt)_3(\mu\text{-}SEt)_3Fe(CN^tBu)_3]$ **2** in good yield (Scheme 1 and Experimental section). The formation of **2** presumably involves asymmetric substitution of ethanethiolate ligands at the bridging-iron centre by the isocyanide and loss of an $\{(SEt)_3MoFe_3S_4(SEt)_3\}$ fragment, the fate of which is unknown. Thermal decomposition of **1** in MeCN in the *absence* of isocyanide gives some of the dicubane $[Mo_2Fe_6S_8$-$(SEt)_9]^{3-}$,[8,9] and this species is occasionally formed as a by-product in the synthesis of the monocubanes.

Compound **2** undergoes classical ligand substitution reactions[1,10,11] at the cubane Fe atoms. Thus reaction of **2** with PhSH affords $[NEt_4][MoFe_3S_4(SPh)_3(\mu\text{-}SEt)_3Fe(CN^tBu)_3]$ **3** and its reaction with PhCOCl gives $[NEt_4][MoFe_3S_4Cl_3$-$(\mu\text{-}SEt)_3Fe(CN^tBu)_3]$ **4**, Scheme 1. The crystal structures of **3** and **4** have been determined by X-ray crystallography, which establish that the new complexes possess an $MoFe_3S_4$ unit bridged *via* three ethanethiolate ligands to an exo-iron atom, the octahedral co-ordination sphere of which is completed by three isocyanide ligands, Figs. 1 and 2. Hitherto, only one other $\{MoFe_3S_4\}$ complex linked to a single exo-metal atom has been structurally characterised, $[NEt_4]_3[MoFe_3S_4(SEt)_3Fe$-$(O_2C_6H_4)_3]$.[7] This species has three bridging O atoms, one from each catecholate ligand, linking the Mo to the Fe atom: the exo-iron atom is suggested to be in a high-spin iron(III) state and this is supported by the Mössbauer spectrum of the analogue $[NEt_4]_3[MoFe_3S_4Cl_3Fe(O_2C_6H_4)_3]$.[11]

For the new complexes **2**, **3** and **4** an important question is what are the oxidation levels associated with the cubane core and the exo-iron centre. Do we have an $\{MoFe_3S_4\}^{3+}$ core linked to an exo-iron(II) unit or an $\{MoFe_3S_4\}^{2+}$ core linked to an exo-iron(III) unit?

Crystallographic data for the cubane assemblies in complexes **3** and **4** are very similar to those found for other complexes with $\{MoFe_3S_4\}$ cores and are unremarkable, Table 1: structural data for known $\{MoFe_3S_4\}^{3+}$ and $\{MoFe_3S_4\}^{2+}$ cores differ only marginally and do not provide a basis for assessing the oxidation levels in the new complexes.[1,4,6–8]

In the parent complex **1** the bridging iron centre is known to be in a low-spin iron(III)[5] state with an Fe–S_{bridge} bond distance of 2.309(9) Å (mean of three).[4] This distance has been shown to increase dramatically by *ca.* 0.2 Å when the iron centre is
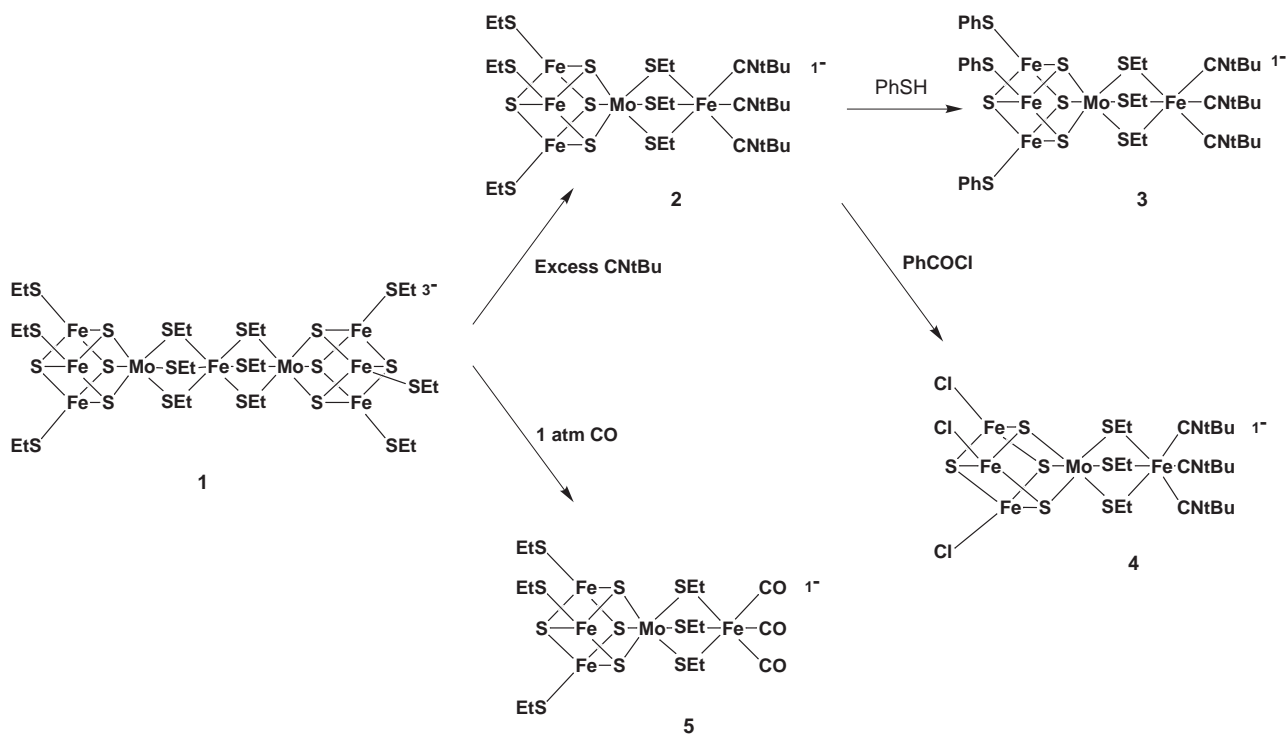
Scheme 1 Reaction of [NEt$_4$]$_3$[Mo$_2$Fe$_7$S$_8$(SEt)$_{12}$] **1** with CN^{t}Bu and CO. Ligand substitution reactions of [NEt$_4$][MoFe$_3$S$_4$(SEt)$_3$(μ-SEt)$_3$Fe(CN-^{t}Bu)$_3$] **2** with PhSH and PhCOCl.
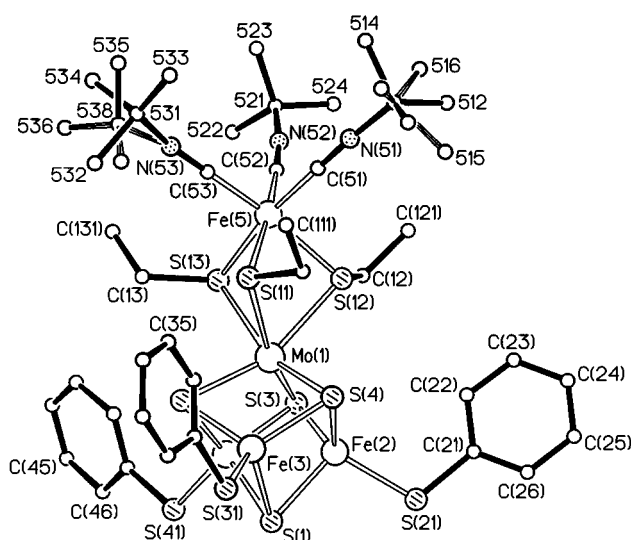
Fig. 1 View of cluster anion [MoFe$_3$S$_4$(SPh)$_3$(μ-SEt)$_3$Fe(CN^{t}Bu)$_3$]$^-$ in compound **3** with the atom labelling indicated.

reduced to the high-spin iron(II) state. We find the Fe–S$_{bridge}$ bond distance in **3** is 2.327(3) Å (mean of three) and in **4** 2.344(4) Å which at first sight suggests the exo-iron atom in these complexes is also low-spin Fe^{III}, Table 1. However, Mössbauer and electrochemical studies definitively show that this is not the case: the exo-iron atom is low-spin Fe^{II} with the cubane unit at the {MoFe$_3$S$_4$}$^{3+}$ oxidation level, see below.

Generally, a relatively small increase in iron–ligand bond length occurs upon reduction of octahedral low-spin Fe^{III} to low-spin Fe^{II}. However, it is becoming clear that if a spin-state change accompanies this process then increases in iron–ligand bond lengths can be quite dramatic, as is observed for the iron-bridged dicubane and as noted for various iron phosphine complexes.[12] Bond length increases associated with spin-state reorganisation have important consequences in electron-transfer kinetics, as is discussed for the parent complex **1** below.

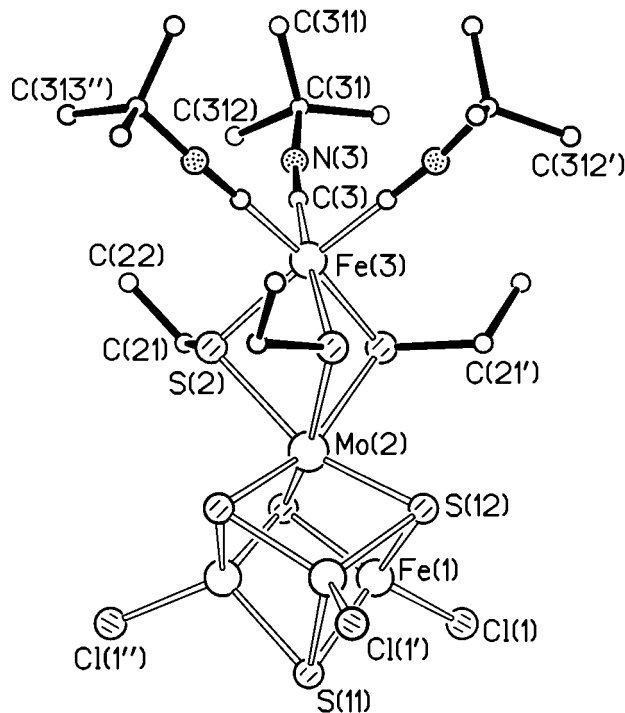**Mössbauer spectroscopy.** The ^{57}Fe Mössbauer parameters for

Fig. 2 View of cluster anion [MoFe$_3$S$_4$Cl$_3$(μ-SEt)$_3$Fe(CN^{t}Bu)$_3$]$^-$ in compound **4** with the atom labelling indicated. A three-fold symmetry axis passes down the length of this ion.

[NEt$_4$][MoFe$_3$S$_4$L$_3$(μ-SEt)$_3$Fe(CN^{t}Bu)$_3$] (L = SEt **2**, SPh **3** or Cl **4**) are listed in Table 2. At 298 K the spectrum of complex **4** shows a quadrupole split doublet superimposed upon a singlet. The 3:1 ratio of intensity of the peaks is fully consistent with assignment of the quadrupole split doublet to the three crystallographically equivalent iron atoms of the cube and the singlet to the exo-iron atom. For cluster **3** the Mössbauer spectrum at 298 K shows two overlapping doublets, relative intensity 2:1, arising from inequivalent cube-iron atoms superimposed upon the singlet of the exo-iron atom (at room temperature there is no crystallographic symmetry in this molecule).

Table 1 Selected molecular dimensions in complexes **3** and **4**. Bond lengths are in Ångströms, angles in degrees. For **3**, all values are means, with s.d.s in parentheses; for **4**, mean values are denoted with an asterisk; e.s.d.s (or s.d.s) are in parentheses

	Complex **3**		Complex **4**	
	Fe(2,3,4)···Fe(3,4,2)	2.694(12)	Fe(1)···Fe(1′)	2.724(4)
	Fe(2,3,4)···Mo(1)	2.717(4)	Fe(1)···Mo(2)	2.707(2)
	Mo(1)···Fe(5)	3.3663(6)	Mo(2)···Fe(3)	3.350(4)
	Fe(2,3,4)–S(1)	2.263(13)	Fe(1)–S(11)	2.298(6)
	Fe(2,3,4)–S(21,31,41)	2.253(3)	Fe(1)–Cl(1)	2.194(5)
	Fe(2,3,4)–S(3,4,2)	2.263(4)	Fe(1)–S(12)	2.251(3)*
	S(2,3,4)–Mo(1)	2.356(4)	S(12)–Mo(2)	2.337(4)
	Mo(1)–S(11,12,13)	2.551(2)	Mo(2)–S(2)	2.540(4)
	S(11,12,13)–Fe(5)	2.327(3)	S(2)–Fe(3)	2.344(4)
	Fe(5)–C(51,52,53)	1.844(2)	Fe(3)–C(3)	1.830(16)
	Fe(2,3,4)–S(1)–Fe(3,4,2)	73.0(6)	Fe(1)–S(11)–Fe(1′)	72.7(2)
	S(1)–Fe(2,3,4)–S(21,31,41)	103.6(13)	Cl(1)–Fe(1)–S(11)	112.0(2)
	S(21,31,41)–Fe(2,3,4)–S(3,4,2)	117.0(6)	Cl(1)–Fe(1)–S(12)	114.0(1)*
	S(1)–Fe(2,3,4)–S(3,4,2)	104.0(5)	S(11)–Fe(1)–S(12)	103.5(1)*
	S(2,3,4)–Fe(3,4,2)–S(4,2,3)	109.11(5)	S(12)–Fe(1)–S(12′)	108.8(2)
	Fe(2,3,4)–S(3,4,2)–Fe(4,2,3)	73.1(4)	Fe(1)–S(12)–Fe(1′)	74.4(2)
	Fe(2,3,4)–S(3,4,2)–Mo(1)	72.0(1)	Fe(1)–S(12)–Mo(2)	72.25(5)*
	S(2,3,4)–Mo(1)–S(3,4,2)	102.94(5)	S(12)–Mo(2)–S(12′)	103.1(2)
	S(11,12,13)–Mo(1)–S(12,13,11)	73.4(2)	S(2)–Mo(2)–S(2′)	74.4(1)
	Mo(1)–S(11,12,13)–Fe(5)	87.15(9)	Mo(2)–S(2)–Fe(3)	86.5(1)
	S(11,12,13)–Fe(5)–S(12,13,11)	82.0(3)	S(2)–Fe(3)–S(2′)	81.9(2)
	C(51,52,53)–Fe(5)–C(52,53,51)	91.1(7)	C(3)–Fe(3)–C(3′)	89.8(6)

Table 2 Mössbauer data for complexes **2**, **3** and **4**

Complex	T/K	Cube iron site(s)			Low spin iron(II) site		
		i.s./mm s^{-1}	q.s./mm s^{-1}	Ratio	i.s./mm s^{-1}	q.s./mm s^{-1}	Ratio
2							
solid state	77	0.52(2)	1.14(3)	2	−0.16	0.22(5)	1
		0.51	0.60(3)	1			
3							
solid state	298	0.52(2)	0.49(3)	1	−0.19	0	1
		0.40(2)	0.95(2)	2			
solid state	77	0.58	0.59	1	−0.28	0.12(2)	1
		0.54	1.19	2			
frozen dmso	77	0.54	0.77(2)	3	−0.09	0	1
4							
	298	0.42	0.49	3	0.02	0	1
solid state	77	0.56	0.92(3)	1	0.05	0	1
		0.54	0.58	2			
frozen dmso	77	0.57	0.66	3	0.02	0	1

Errors ≤0.01 mm s^{-1} unless otherwise stated. Half-widths at half maxima are in the range 0.13–0.24 mm s^{-1}.

The isomer shifts (i.s.) for the cube irons of complexes **2**, **3** and **4** are in the range expected for iron atoms of the $\{MoFe_3S_4\}^{3+}$ core.[5,7–9,11,13] Importantly, the Mössbauer parameters of **3** exhibit the expected variation with temperature; both the i.s. and q.s. (quadrupole splitting) of the cube-iron atoms increase with decrease in temperature. The absorbance of the exo-iron atom shows a small increase in shift with decrease in temperature and at 77 K also shows a small splitting; this is fully consistent with a low-spin iron(II) centre.

Interestingly, the cluster **4** shows an unexpected, abrupt change in the Mössbauer spectrum at ≈145–150 K. Below this temperature the cube-iron atoms become inequivalent in a ratio of 2:1. The i.s. of the exo-iron(II) singlet changes only slightly over the temperature range studied. When **4** is dissolved in dimethyl sulfoxide (dmso), to disrupt the crystallographic lattice, and the solution rapidly frozen, the resultant spectrum at 77 K shows the cube-iron atoms again to be equivalent. The parameters for the cube irons are similar to those predicted by extrapolation of the data, obtained in the solid state above 150 K, to 77 K assuming that the cube-iron atoms remain equivalent (predicted i.s. = 0.57; q.s. = 0.67 mm s^{-1}). The same effect is observed when **3** is dissolved in dmso; the cube-iron atoms become equivalent, corresponding to the crystallographic lattice being disrupted.

Previously it has been observed that the spectrum of the salt [NEt$_3$CH$_2$Ph]$_3$[Mo$_2$Fe$_6$S$_8$(SEt)$_9$] at 77 K shows two overlapping doublets, indicating inequivalent iron atoms, inconsistent with the equivalence of the iron atoms in the structure determined at room temperature.[8] The related salt [NEt$_4$]$_3$[Mo$_2$Fe$_6$S$_8$(SPh)$_9$] also shows inequivalent iron atoms in both the solid and frozen solution Mössbauer spectrum.[9] In neither case was an origin of the effect proposed.

These earlier and the present observations can be rationalised if it is accepted that the inequivalence of the cube-iron atoms arises due to asymmetry of the crystalline lattice. Thus we propose that the crystal lattice of complex **4** is symmetrical above 145–150 K; around this temperature a reversible solid state change occurs and below it the lattice becomes asymmetric and the cube-iron atoms inequivalent. In support of this we find that on dissolution of **4** in dmso at 298 K followed by rapid freezing and cooling to 77 K the cube-iron atoms are found to be all *equivalent*. Cluster **3** has a lattice with no symmetry at room temperature and the cube-iron atoms remain inequivalent over the temperature range, 77–298 K, studied.

Table 3 Redox potentials and infrared data for complexes **2**, **3**, **4** and **5**

Complex	Reduction and oxidation potential (V)	FT-IR (cm^{-1})
5	$E_{\frac{1}{2}}^{\mathrm{red}}$ −1.69, $E_{\mathrm{p}}^{\mathrm{ox}}$ −0.59	ν(CO) 1958, 1993
2	$E_{\frac{1}{2}}^{\mathrm{red}}$ −1.71, $E_{\mathrm{p}}^{\mathrm{ox}}$ −0.59	ν(CN) 2117, 2159
3	$E_{\frac{1}{2}}^{\mathrm{red1}}$ −1.47, $E_{\frac{1}{2}}^{\mathrm{ox}}$ −0.42	ν(CN) 2119, 2161
	$E_{\frac{1}{2}}^{\mathrm{red2}}$ −2.43*	
4	$E_{\frac{1}{2}}^{\mathrm{red1}}$ −1.32, $E_{\frac{1}{2}}^{\mathrm{ox}}$ −0.07	ν(CN) 2122, 2163
	$E_{\frac{1}{2}}^{\mathrm{red2}}$ −2.25*	

Redox potentials (*: recorded at −15 °C) were measured in MeCN–0.2 M [NBu$_4$][BF$_4$] electrolyte at a glassy-carbon working electrode, potentials are given *versus* the ferrocenium–ferrocene couple. FT-IR measurements were made in solution in MeCN.
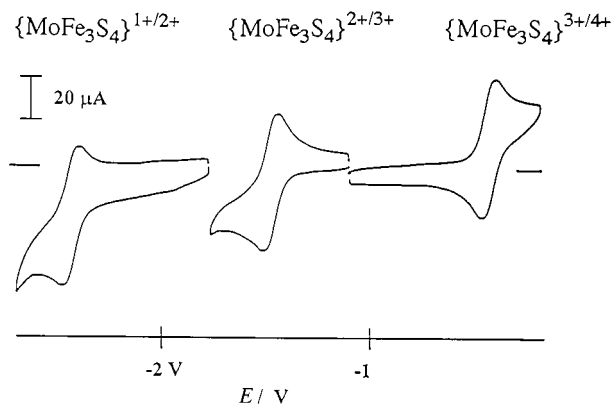

Fig. 3 Electron transfer series of [MoFe$_3$S$_4$(SPh)$_3$(μ-SEt)$_3$Fe(CN-$^{\mathrm{t}}$Bu)$_3$]$^{0/1-/2-/3-}$ in MeCN–0.2 M [NBu$_4$][BF$_4$] at −15 °C. Potentials are *versus* the ferrocenium–ferrocene couple. The scan rate is 200 mV s^{-1}.

However, dissolution of **3** in dmso at 298 K disrupts the lattice and the cube-iron atoms are now seen to be equivalent at 77 K.

Electrochemistry

Monocubanes with exo-iron centres. The cyclic voltammetry of the monocubane complex **3** in MeCN–0.2 M [NBu$_4$][BF$_4$] at a vitreous carbon electrode at low temperature is shown in Fig. 3. The primary electron-transfer reactions of the cluster are a reversible one-electron reduction and a reversible one-electron oxidation. The potential domains in which these primary processes occur are close to those associated with the {MoFe$_3$S$_4$}$^{3+/2+}$ and {MoFe$_3$S$_4$}$^{4+/3+}$ couples in other cubane and dicubane systems.[1,4,7,9] That these processes are cubane-based is also supported by the following evidence. Formal replacement of the cubane PhS$^-$ ligands by EtS$^-$ or by Cl$^-$ has the expected large effect on the primary redox potentials,[1,10] Table 3. Thus changing the cube EtS$^-$ ligand to more electron-withdrawing ligands, PhS$^-$ or Cl$^-$, shifts the potentials to positive values by +240 and +390 mV respectively for the primary reduction and +170 and +520 mV respectively, for the primary oxidation, indicative of a large electron density change at the cube redox site. Conversely, replacing the isocyanide ligands on the exo-Fe atom in complex **2** by CO, complex **5**, is found to have a *negligible effect* on $E°$ for these processes, Table 3: if either primary redox step were associated with the exo-iron a considerable shift in $E°$ should be observed.[14]

The isocyanide IR stretching frequency, ν(CN), in co-ordination compounds is generally a reasonably sensitive probe of changes in the electronic condition of the metal centre to which it is bound.[15] For example, factors which decrease electron density on the metal such as oxidation or introduction of an electron-withdrawing group shift ν(CN) to lower energies. Table 3 lists ν(CN) for the new complexes. Despite large
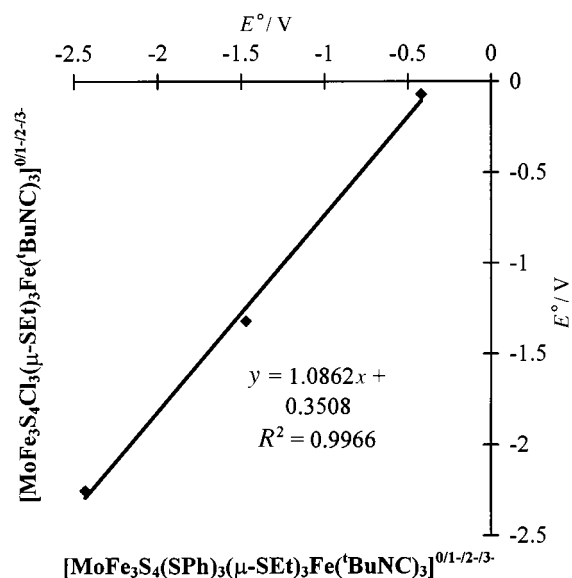
Fig. 4 Plot of $E°$ potentials (V) for the two series [MoFe$_3$S$_4$(X)$_3$-(μ-SEt)$_3$Fe(CN$^{\mathrm{t}}$Bu)$_3$]$^{0/1-/2-/3-}$ (X = SPh or Cl) with substituted {MoFe$_3$S$_4$} cubane cores.

changes in $E°$ potentials consequent upon cubane-ligand substitution, the isocyanide stretching frequency is essentially unchanged. This strongly suggests that the cubane and the exo-iron(II) site are *electronically insulated* from one another. As noted above, [NEt$_4$][MoFe$_3$S$_4$(SEt)$_3$(μ-SEt)$_3$Fe(CO)$_3$] **5** and **2** have essentially identical primary $E°$ potentials, despite formal replacement of the isocyanide by the strongly electron-accepting CO ligand: the {Mo(μ-SR)$_3$Fe} unit appears ineffectual in transmitting substituent effects between the cubane and the exo-iron centre.

Complicated secondary oxidation processes are observed beyond the primary cubane based oxidation of complexes **2**–**5**; these are probably associated with irreversible oxidation of the exo-iron centre and/or degradation of the cubane core and will not be considered further.

More importantly, low temperature cyclic voltammetry shows that a secondary *reversible* one-electron reduction step is observed for complex **3** at a potential which is about 1 V negative of the primary reversible reduction, Fig. 3. This reduction process is shifted 200 mV positive for the chloro-complex **4**, as is consistent with cubane-based electron transfer. The detection of the hitherto unobserved monocubane {MoFe$_3$S$_4$}$^{2+/1+}$ couple now completes a four membered electron-transfer series {MoFe$_3$S$_4$}$^{4+/3+/2+/1+}$ which complements that of the *all-iron* {Fe$_4$S$_4$}$^{3+/2+/1+/0}$ cubane series.[16] Fig. 4 shows the expected linear plot of $E°$ potentials for the chloro-substituted {MoFe$_3$S$_4$} series *versus* those of the corresponding thiophenolate {MoFe$_3$S$_4$} series (correlation coefficient, $R = 0.998$). The slope is slightly greater than unity (1.1) and this is presumably indicative of the harder nature of the chloride *vis-à-vis* the thiophenolate ligands: *i.e.* chloride is less effective in releasing electron density onto the {MoFe$_3$S$_4$} core, to compensate for charge removed by oxidation, than is thiolate.

There is a close correspondence between the redox manifolds of the all-iron and the molybdenum-iron cluster sets. Fig. 5 shows the plot of $E°$ potentials for the {MoFe$_3$S$_4$}$^{4+/3+/2+/1+}$ series *versus* those for the {Fe$_4$S$_4$}$^{3+/2+/1+/0}$ series; the cubane Fe atoms are co-ordinated by thiophenolate in both series. The linear plot has a slope close to unity with $E°$'s for each {MoFe$_3$S$_4$}$^{(n+1)+}$ member displaced by about −200 mV from the corresponding {Fe$_4$S$_4$}$^{n+}$ member. Thus upon formally replacing an iron(II) centre in {Fe$_4$S$_4$}$^{2+}$ by a molybdenum(III) centre the resulting cubane becomes somewhat more electron-rich, despite the increase in one unit of positive charge on the core, and the lower d-electron count (19 electrons for the
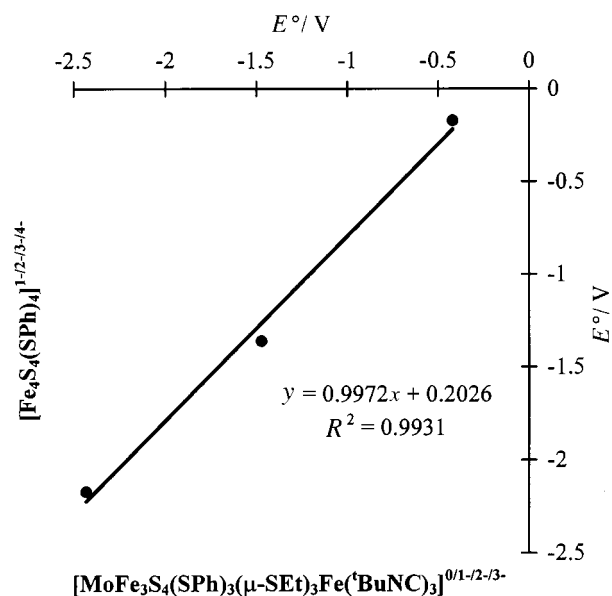
Fig. 5 Plot of $E°$ potentials (V) for the two series of thiophenolate substituted cubane cores: $[MoFe_3S_4(SPh)_3(\mu\text{-}SEt)_3Fe(CN^tBu)_3]^{0/1-/2-/3-}$ and $[Fe_4S_4(SPh)_4]^{1-/2-/3-/4-}$.

$\{MoFe_3S_4\}^{3+}$ core *versus* 22 for $\{Fe_4S_4\}^{2+}$).† A similar trend in the two chloro substituted series is observed, however the linear correlation is less good (correlation coefficients are 0.997 and 0.976 for the thiophenolate and chloro-series respectively).

The iron-bridged dicubane system: electron transfer involving the bridging-iron unit. Reductive cyclic voltammograms of complex **1** at 293 and 243 K (vitreous carbon; 0.2 M $[NBu_4][BF_4]$–MeCN) are shown in Fig. 6. The primary process observed at 293 K corresponds to the reversible reduction of the bridging iron(III) centre.[5] The electron-transfer dynamics of this process is slow. Thus the peak potential separation, $\Delta E = E_p^{ox} - E_p^{red}$, (i) increases with increasing scan rate and (ii) increases as the temperature is lowered: both responses are indicative of a quasi-reversible process. For example: ΔE increases from $\Delta E_{293K} = 80$ mV to $\Delta E_{243K} = 270$ mV.‡ The standard heterogeneous rate constant, k^0_s, for reversible electron transfer to the bridging iron centre can be estimated from ΔE, and the variation of k^0_s with temperature allows calculation of the activation energy, E_a, associated with this process. Digital simulation of the cyclic voltammetric response for the bridging $Fe^{III,II}$ system gives $k^0_{s(293\ K)} = (3 \pm 2) \times 10^{-3}$ cm s^{-1} and $E_a = 36 \pm 3$ kJ mol^{-1}, Fig. 7.

Slow electron-transfer chemistry (quasi-reversibility) is usually associated with a large structural[18] and/or spin-state reorganisational energy barrier.[19] Crystal structural data have shown that in bridging $\{(RS)_3Fe(SR)_3\}$ units the Fe–S bond lengths *increase* by an average of 0.2 Å upon reduction of Fe^{III} to Fe^{II},[4] indicative of a considerable structural reorganisation, in addition Mössbauer data indicate that upon reduction the spin state changes from low (t_{2g}^5) to high $(t_{2g}^4\ e_g^2)$.[5] Both structural and spin-state changes are consistent with the observed quasi-reversibility of the Fe^{III}–Fe^{II} couple.

---

† Strictly this is replacing $\{Mo(\mu\text{-}SEt)_3Fe(CN^tBu)_3\}^{3+}$ by $\{Fe^{II}(SPh)\}^{2+}$ at an $\{Fe_3S_4(SPh)_3\}^0$ assembly.[1]

‡ These results are not a consequence of uncompensated solution resistance because under the same experimental conditions ΔE for the subsequent reversible processes associated with reduction of the cubane centres are close to the theoretical values for fast heterogeneous electron transfer.

The simulations were carried out using DIGISIM 2.0.[17] The asymmetry of the $Fe^{III,II}$ voltammetric response (Fig. 7) was accommodated when the electron-transfer coefficient, a, was 0.4.
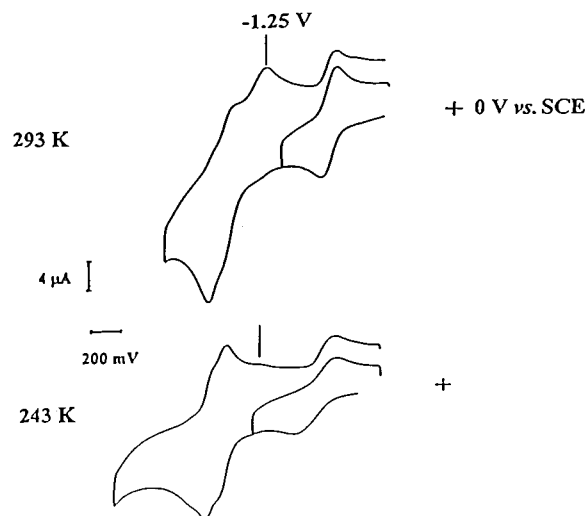

Fig. 6 Reductive voltammograms of complex **1** at 293 and 243 K. Potentials are *versus* SCE. The scan rate is 200 mV s^{-1}.

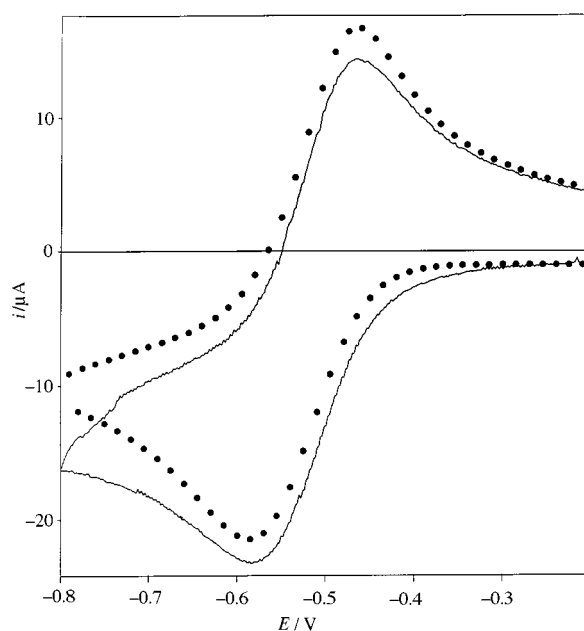**Fig. 7** Experimental and digital simulation (●) of the cyclic voltammetric response for the bridging $Fe^{III,II}$ system in complex **1**. The scan rate is 200 mV s^{-1}.

Electron-transfer involving the cubane centres. The cyclic voltammograms in Fig. 6 show that, following reduction of the bridging iron-unit, further reversible electron-transfer chemistry takes place at more negative potentials. The voltammogram at 243 K is particularly instructive: two overlapping, but otherwise well resolved, reversible one-electron transfer steps are observed in a potential domain typical of $\{MoFe_3\text{-}S_4\}^{3+}$ cubane cores. The peak separations $\{E_p^{ox} - E_p^{red}\}$ for both electron-transfer steps are close to the theoretical value (48 mV) for a reversible one-electron transfer at 243 K. The $E°$ potentials for the two successive reduction steps differ by $\Delta E° = 90 \pm 10$ mV. This is greater than the statistical value of 36 mV that would be expected if electronic communication between the cubane centres were negligible. The magnitude of $\Delta E°$ corresponds to a comproportionation constant, $K_{com(243K)} = 80 \pm 30$, and is indicative of weak interaction between the cubane sub-sites.

The two successive reversible one-electron reduction processes observed at 243 K become partially reversible as the temperature is increased and this is accompanied by the appearance of a new reversible system near −1.25 V *versus* the saturated

calomel electrode (SCE). Single and repetitive scanning cyclic voltammetry suggests that the system involves redox-linked equilibria associated with interconverting forms of the dicubane system, Fig. 8. Thus the principal features of the voltammetry can be accommodated by the model "scheme of squares" shown in Scheme 2. Simulated voltammograms based on this model are shown in Fig. 8. The experimental data have somewhat broader features than do the simulated data; this may arise from a range of different conformation states with close, but non-identical, redox properties.

We cannot definitively establish the structural rearrangements which take place following electron transfer at ambient temperature because the redox isomers are not stable on the preparative timescale. However, we can offer some insight into the chemistry involved which is based on the following experimental observations. (i) There is a decrease in the effective charge on the cubane cores since the potentials associated with oxidation of the reorganised system are shifted positive by *ca.* 100 mV. (ii) As the charge on the system is increased, the isomerism of $\mathbf{1}^{n-}$ becomes thermodynamically and kinetically more favourable. (iii) The molybdenum centre is directly involved in the structural isomerism because the analogous tungsten sys-
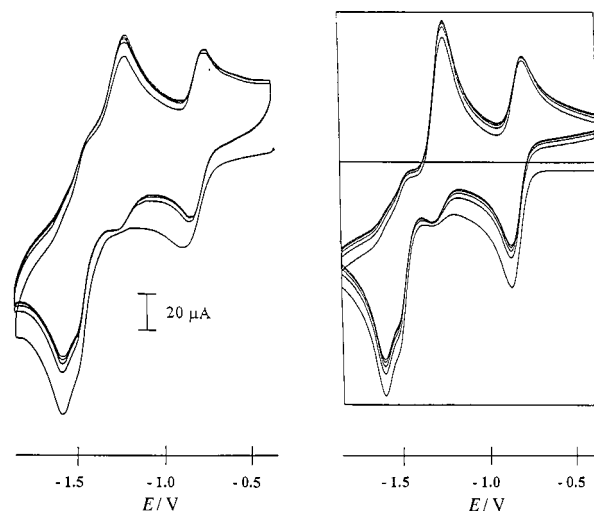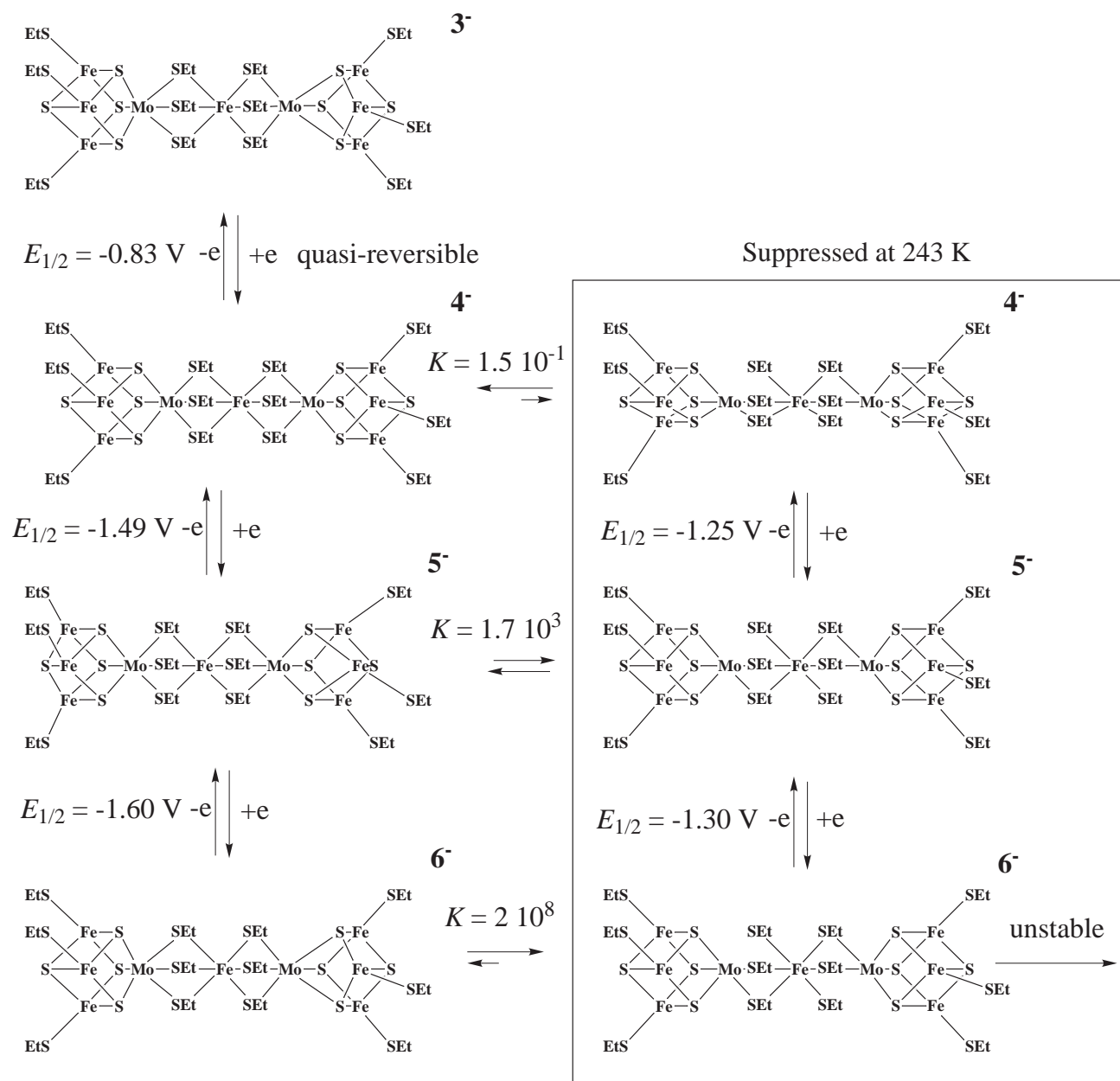

Fig. 8 Experimental (left) and digital simulation (right) of the reductive cyclic voltammetric response for complex **1**. Five successive cycles are shown. The scan rate is 200 mV s^{-1}.

Scheme 2 Proposed mechanism for the redox transformations of complex **1**, based on the simulation data.

tem behaves at room temperature[5] in much the same way as does the molybdenum system at low temperature: *i.e.* uncomplicated, successive, single electron-transfer steps. This is consistent with lower ligand lability at W relative to Mo, a general feature of the comparative chemistry of these two metals. The positive shift in redox potentials, the relatively "fast" chemistry of the molybdenum system and the dependence of the equilibria and rates on the total charge on the system can be accommodated by reversible deco-ordination of a bridging thiolate ligand from a molybdenum cubane centre as is suggested in Scheme 2. There is chemical precedence for such a step in the reversible opening of a thiolate bridge between dimolybdenum centres following electron transfer.[20]

Conclusion

Cubane clusters with exo-iron atoms can be synthesized from the iron-bridged dicubane $[NEt_4]_3[Mo_2Fe_7S_8(SEt)_{12}]$ **1** by reactions with π-acid ligands. The structures of two isocyanide derivatives have been established by X-ray crystallography. Electrochemical and Mössbauer data show that the cubane core retains the $\{MoFe_3S_4\}^{3+}$ redox level of the parent material **1** and that the exo-iron centre is in the low-spin iron(II) state. Infrared and electrochemical data show that there is little electronic interaction between the cubane and exo-iron centres. The parent complex **1** possesses a low-spin bridging iron(III) centre. This centre undergoes slow electron transfer which is ascribed to spin-state reorganisation to high-spin Fe^{II}. Reduction of the cubane units leads to reversible deco-ordination of a bridging thiolate group from a molybdenum centre.

Experimental

General

All manipulations were carried out under an inert atmosphere of dinitrogen or argon using Schlenk techniques. Solvents were freshly distilled from appropriate drying agents under dinitrogen. The NMR measurements were made on a JEOL GSX270 or JNM-LA400 instrument at room temperature. Infrared spectra were recorded on a Bio-Rad spectrometer coupled to Win-IR software or using a Perkin-Elmer 883 spectrometer. Mössbauer spectra were recorded at 77–298 K on an ES-Technology MS-105 spectrometer with a 925 MBq ^{57}Co source in a rhodium matrix at ambient temperature, referenced to a 25 μm iron foil at 298 K. Frozen dimethyl sulfoxide solution samples were prepared as described elsewhere[21] with a cluster salt concentration of approximately 25 mM.

Cyclic voltammetric experiments were carried out using a Hi-Tek DT 2101 potentiostat interfaced with a Hi-Tek PP RI waveform generator with output recorded on a Philips PM 8041 X-Y recorder or on a computer controlled EG and G PAR model 273 potentiostat running EG and G PAR M270 and DIGISIM 2.0 software.

Microanalyses were carried out either at the Department of Chemical Sciences, University of East Anglia or at the Centre de Microanalyses du CNRS, Vernaison. Sulfur analyses were problematic, but this is not uncommon for iron–sulfur clusters.

Crystal structure analyses of $[NEt_4][MoFe_3S_4X_3(\mu-SEt)_3-Fe(CN^tBu)_3]$ (X = SPh or Cl)

Crystal data for $[NEt_4][MoFe_3S_4(SPh)_3(\mu-SEt)_3Fe(CN^tBu)_3]$ 3. Triclinic, space group $P\bar{1}$ (no. 2), $a = 12.557(1)$, $b = 13.711(1)$, $c = 19.494(2)$ Å, $\alpha = 99.835(8)$, $\beta = 87.427(8)$, $\gamma = 107.024(8)°$, $U = 3162.1(6)$ Å^3, $T = 293(1)$ K, $Z = 2$, $D_c = 1.405$ g cm^{-3}, μ(Mo-Kα) = 14.5 cm^{-1}, $R1$[22] = 0.064 and $wR2$[22] = 0.118 for all 11097 reflections and 590 parameters; for the 7829 reflections having $I > 2\sigma_I$, $R1 = 0.041$.

Crystal data for $[NEt_4][MoFe_3S_4Cl_3(\mu-SEt)_3Fe(CN^tBu)_3]\cdot$MeCN 4. Trigonal, space group $P3_1c$ (no. 159), $a = b =$

11.255(2), $c = 23.878(3)$ Å, $U = 2618.9(10)$ Å^3, $T = 293(1)$ K, $Z = 2$, $D_c = 1.468$ g cm^{-3}, μ(Mo-Kα) = 17.6 cm^{-1}, R[23] = 0.098 and R'[23] = 0.083 for all 1554 reflections and 161 parameters; for the 804 reflections having $I > \sigma_I$, $R = 0.051$.

The deep red crystals of $[NEt_4][MoFe_3S_4(SPh)_3(\mu-SEt)_3-Fe(CN^tBu)_3]$ **3** and $[NEt_4][MoFe_3S_4Cl_3(\mu-SEt)_3Fe(CN^tBu)_3]\cdot$MeCN **4** were mounted on glass fibres and **3** was coated with epoxy resin. After preliminary photographic examination, they were transferred to an Enraf-Nonius CAD4 diffractometer (with monochromated Mo-Kα radiation, $\lambda = 0.71069$ Å) for determination of accurate cell parameters (from the setting of 25 reflections, $\theta = 10–11$ and $8–10°$ respectively, each reflection centred in four orientations) and for measurement of diffraction intensities using an $\omega–\theta$ scan mode for **3** and an $\omega–2\theta/3$ scan mode for **4**; for both crystals, data were recorded for the θ range 1.5–25°. During processing, corrections were applied for Lorentz-polarisation effects, absorption (by semiempirical ψ-scan methods) and to eliminate negative net intensities (by Bayesian statistical methods). A small deterioration correction was applied for **4**; none was necessary for **3**.

The structure of complex **3** was determined by the automated Patterson routines in the SHELXS program[24] and refined by full-matrix least-squares methods, initially on F in SHELX and SHELXN,[23] finally on F^2 in SHELXL.[22] Two of the isocyanide ligands showed disorder in the *tert*-butyl group positions. Except in these groups, hydrogen atoms were included in idealised positions. The non-hydrogen atoms (except for the disordered carbons atoms) were refined with anisotropic thermal parameters and the H-atom U_{iso} values were set to ride on the U_{eq} values of the parent carbon atoms.

The data collected for complex **4** were input to the SHELX[23] system. An M_4S_4 cubane type moiety, lying on a threefold symmetry axis, was identified in an E map generated by the direct methods procedures in SHELXS,[24] and the remainder of the structure was found in successive electron density and Fourier difference maps. The anion is well defined and its non-hydrogen atoms were allowed anisotropic thermal parameters. Hydrogen atoms were included in idealised positions on the ethanethiolate ligand (the methyl group in a staggered orientation) with positional and thermal parameters riding on those of the parent carbon atoms. The cation is not fully resolved; it lies disordered about a second 3-fold axis. A solvent molecule lies along the first symmetry axis. Refinement of the structure with reversed polarity showed no significant differences in R values or molecular dimensions.

For both structures, scattering factor curves for neutral atoms were taken from ref. 25. Computer programs used in these analyses have been noted above or in Table 4 of ref. 26 and were run on the DEC-Alpha machine in the Nitrogen Fixation Laboratory.

CCDC reference number 186/1344.

See http://www.rsc.org/suppdata/dt/1999/957/ for crystallographic files in cif. format.

Syntheses

The salt $[NEt_4]_3[Mo_2Fe_7S_8(SEt)_{12}]$ **1** was made as reported in the literature.[4,5]

$[NEt_4][MoFe_3S_4(SEt)_3(\mu-SEt)_3Fe(CN^tBu)_3]$ 2. The salt $[NEt_4]_3[Mo_2Fe_7S_8(SEt)_{12}]$ **1**, 0.55 g (0.28 mmol), was dissolved in MeCN, 50 mL. To this solution was added an excess of CN^{t}Bu (0.19 mL, 1.68 mmol, 6 equivalents). The solution was stirred for 10 d under N$_2$. After addition of Et$_2$O, 20 mL, the solution was stored at -14 °C for 2 h, filtered, and the filtrate then taken to dryness under vacuum. The salt $[NEt_4]$-$[MoFe_3S_4(SEt)_3(\mu-SEt)_3Fe(CN^tBu)_3]$ **2**, 0.3 g (90%), was obtained as a black glassy powder. Attempts to shorten the reaction time by working at elevated temperatures tended to lead to the formation of $[NEt_4]_3[Mo_2Fe_6S_8(SEt)_9]$ and precipit-

ation of insoluble, intractable solids (Found: C, 35.12; H, 6.64; N, 5.1; S, 17.4. Calc. for $C_{35}H_{77}Fe_4MoN_4S_{10}$: C, 35.21; H, 6.50; N, 4.69; S, 26.85%). ^1H NMR (CD_3CN): δ 55.14 (CH_2 in SEt, broad), 8.40 (CH_2 in μ-SEt, broad), 7.00 (CH_3 in SEt, very broad), 4.35 (CH_3 in μ-SEt, broad), 3.21 (CH_2 in NEt_4), 1.56 (CN^tBu) and 1.27 (CH_3 in NEt_4). FT-IR (in MeCN): ν(CN) 2117 and 2159 cm^{-1}.

[NEt₄][MoFe₃S₄(SPh)₃(μ-SEt)₃Fe(CNᵗBu)₃] 3. The salt $[NEt_4]_3[Mo_2Fe_7S_8(SEt)_{12}]$ **1**, 0.86 g (0.44 mmol), was dissolved in MeCN, 50 mL, and CN^tBu, 0.30 mL (2.63 mmol), was added. The solution was stirred for 10 d under N_2, PhSH, 0.36 mL (3.50 mmol), was added and the yellow-black solution turned instantly to dark red. After 15 min of stirring about 20 mL of Et_2O were added and the solution then kept for 2 h at -14 °C. It was filtered, the filtrate reduced to 20 mL under vacuum and ethyl acetate, 30 mL, added. This solution was kept overnight at -14 °C, filtered and the precipitate dried under vacuum to give $[NEt_4][MoFe_3S_4(SPh)_3(\mu\text{-}SEt)_3Fe(CN^tBu)_3]$ **3**, 0.35 g (60%), as a black glassy powder. The filtrate was kept at room temperature and very dark, deep red octahedral crystals of $[NEt_4][MoFe_3S_4(SPh)_3(\mu\text{-}SEt)_3Fe(CN^tBu)_3]$ **3** appeared within a few hours (Found: C, 43.42; H, 6.00; N, 4.4; S, 25.8. Calc. for $C_{47}H_{77}Fe_4MoN_4S_{10}$: C, 42.19; H, 5.80; N, 4.19; S, 23.96%). ^1H NMR (CD_3CN): δ 22.96 (o-, m- or p-H in SPh, broad), 13.73 (CH_2 in μ-SEt, broad), 7.31 (CH_3 in μ-SEt, broad), 3.15 (CH_2 in NEt_4), 1.56 (CN^tBu), 1.21 (CH_3 in NEt_4), -3.63 (o-, m- or p-H in SPh, broad) and -24.35 (o-, m- or p-H in SPh, broad). FT-IR (in MeCN): ν(CN) 2119 and 2161 cm^{-1}.

[NEt₄][MoFe₃S₄Cl₃(μ-SEt)₃Fe(CNᵗBu)₃]·MeCN 4. The salt $[NEt_4]_3[Mo_2Fe_7S_8(SEt)_{12}]$ **1**, 1.15 g (0.59 mmol), was dissolved in MeCN, 110 mL, and CN^tBu, 0.4 mL (3.51 mmol), was added. The solution was stirred for 10 d under N_2, PhCOCl, 0.55 mL (4.69 mmol), was added and the yellow-black solution turned instantly to dark brown. After 15 min of stirring the solution was concentrated under vacuum at 80 °C until crystals began to appear. The solution was then allowed to cool to room temperature affording black crystals of $[NEt_4][MoFe_3S_4Cl_3(\mu\text{-}SEt)_3Fe(CN^tBu)_3]\cdot MeCN$ **4**, 0.42 g (62%) (Found: C, 32.25; H, 5.60; Cl, 9.11; N, 5.9. Calc. for $C_{31}H_{65}Cl_3Fe_4MoN_5S_7$: C, 32.15; H, 5.66; Cl, 9.18; N, 6.05%). ^1H NMR (CD_3CN): δ 11.50 (CH_2 in μ-SEt), 7.60 (CH_3 in μ-SEt), 3.15 (CH_2 in NEt_4), 1.53 (CN^tBu) and 1.21 (CH_3 in NEt_4). FT-IR (in MeCN): ν(CN) 2122 and 2163 cm^{-1}. IR (CsI pellet): ν(FeCl) 353 cm^{-1}.

Generation of [NEt₄][MoFe₃S₄(SEt)₃(μ-SEt)₃Fe(CO)₃] 5. The salt $[NEt_4]_3[Mo_2Fe_7S_8(SEt)_{12}]$ **1**, 0.30 g, was dissolved in MeCN, 100 mL, and stirred for 15 d under 1 atm of CO. The complex $[NEt_4][MoFe_3S_4(SEt)_3(\mu\text{-}SEt)_3Fe(CO)_3]$ **5** was obtained in solution and characterised by its FT-IR ν(CO) bands (1958, 1993 cm^{-1} in MeCN) and by comparison of its redox potentials with those of the isocyanide analogue **2** (Table 3).

Acknowledgements

References

1 R. H. Holm, *Chem. Soc. Rev.*, 1981, **10**, 455; R. H. Holm and E. D. Simhon, in *Molybdenum Enzymes*, ed. T. G. Spiro, Wiley (Interscience), New York, 1985, ch. 1, pp. 1–87; R. H. Holm, *Adv. Inorg. Chem.*, 1992, **38**, 1.
2 R. H. Holm, P. Kennepohl and E. I. Solomon, *Chem. Rev.*, 1996, **96**, 2239.
3 J. Kim and D. C. Rees, *Science*, 1992, **257**, 1677; S. W. Ragsdale and M. Kumar, *Chem. Rev.*, 1996, **96**, 2515; A. Volbeda, M. H. Charon, C. Piras, E. C. Hatchikian, M. Frey and J. C. Fontecilla-Camps, *Nature* (*London*), 1995, **373**, 580; R. P. Happe, W. Rosenboom, A. J. Pierik, S. P. J. Albracht and K. A. Bagley, *Nature* (*London*), 1997, **385**, 126.
4 T. E. Wolff, J. M. Berg, P. P. Power, K. O. Hodgson and R. H. Holm, *Inorg. Chem.*, 1980, **19**, 430.
5 T. E. Wolff, P. P. Power, R. B. Frankel and R. H. Holm, *J. Am. Chem. Soc.*, 1980, **102**, 4694.
6 R. E. Palermo, R. Singh, J. K. Bashkin and R. H. Holm, *J. Am. Chem. Soc.*, 1984, **106**, 2600.
7 T. E. Wolff, J. M. Berg and R. H. Holm, *Inorg. Chem.*, 1981, **20**, 174.
8 T. E. Wolff, J. M. Berg, K. O. Hodgson, R. B. Frankel and R. H. Holm, *J. Am. Chem. Soc.*, 1979, **101**, 4140.
9 G. Christou, P. K. Mascharak, W. H. Armstrong, G. C. Papaefthymiou, R. B. Frankel and R. H. Holm, *J. Am. Chem. Soc.*, 1982, **104**, 2820.
10 R. E. Palermo, P. P. Power and R. H. Holm, *Inorg. Chem.*, 1982, **21**, 173.
11 J. E. Barclay, D. J. Evans, G. J. Leigh and J. B. Parra-Soto, *J. Chem. Soc.*, *Dalton Trans.*, 1993, 543.
12 J. E. Barclay, A. Hills, D. L. Hughes and G. J. Leigh, *J. Chem. Soc.*, *Dalton Trans.*, 1988, 2871.
13 P. K. Mascharak, G. C. Papaefthymiou, W. H. Armstrong, S. Foner, R. B. Frankel and R. H. Holm, *Inorg. Chem.*, 1983, **22**, 2851.
14 J. Chatt, C. T. Kan, G. J. Leigh, C. J. Pickett and D. R. Stanley, *J. Chem. Soc.*, *Dalton Trans.*, 1980, 2032.
15 A. C. Sarapu and R. F. Fenske, *Inorg. Chem.*, 1975, **14**, 247.
16 C. J. Pickett, *J. Chem. Soc.*, *Chem. Commun.*, 1985, 323.
17 M. Rudolph and S. W. Feldberg, DIGISIM 2.0, Bioanalytical Systems, Inc., West Lafayette, IN, 1994.
18 W. E. Geiger, *Prog. Inorg. Chem.*, 1985, **33**, 275; D. H. Evans and K. M. O'Connel, in *Electroanalytical Chemistry*, ed. A. J. Bard, Marcel Dekker, New York, 1986, vol. 14, p. 113; F. A. Schultz, *J. Electroanal. Chem. Interfacial Electrochem.*, 1986, **213**, 169; D. L. Hughes, S. K. Ibrahim, C. J. Pickett, G. Querné, A. Laouénan, J. Talarmin, A. Queiros and A. Fonseca, *Polyhedron*, 1994, **13**, 3341.
19 A. Hammershøi, D. Geselowitz and H. Taube, *Inorg. Chem.*, 1984, **23**, 979.
20 F. Gloaguen, C. Le Floc'h, F. Y. Pétillon, J. Talarmin, M. El Khalifa and J.-Y. Saillard, *Organometallics*, 1991, **10**, 2004.
21 J. E. Barclay, D. J. Evans, G. J. Leigh, M. S. Newton and J. Silver, *Gazz. Chim. Ital.*, 1994, **124**, 367.
22 G. M. Sheldrick, SHELXL, Program for crystal structure refinement, University of Göttingen, 1993.
23 G. M. Sheldrick, SHELX, Program for crystal structure analysis, University of Cambridge, 1976; extended version, SHELXN, 1977.
24 G. M. Sheldrick, *Acta Crystallogr.*, *Sect. A*, 1990, **46**, 467.
25 *International Tables for X-Ray Crystallography*, Kynoch Press, Birmingham, 1974, vol. 4, pp. 99 and 149.
26 S. N. Anderson, R. L. Richards and D. L. Hughes, *J. Chem. Soc.*, *Dalton Trans.*, 1986, 245.

Paper 8/09710K